

1-1-2012

Resonant electron transfer and L-shell excitation for $_{26}\text{Fe}^{19+}$ and $_{30}\text{Zn}^{23+}$ ions

HASSAN RAMADAN

Follow this and additional works at: <https://journals.tubitak.gov.tr/physics>



Part of the [Physics Commons](#)

Recommended Citation

RAMADAN, HASSAN (2012) "Resonant electron transfer and L-shell excitation for $_{26}\text{Fe}^{19+}$ and $_{30}\text{Zn}^{23+}$ ions," *Turkish Journal of Physics*: Vol. 36: No. 1, Article 12. <https://doi.org/10.3906/fiz-1012-60>

Available at: <https://journals.tubitak.gov.tr/physics/vol36/iss1/12>

This Article is brought to you for free and open access by TÜBİTAK Academic Journals. It has been accepted for inclusion in Turkish Journal of Physics by an authorized editor of TÜBİTAK Academic Journals. For more information, please contact academic.publications@tubitak.gov.tr.

Resonant electron transfer and L-shell excitation for ${}_{26}\text{Fe}^{19+}$ and ${}_{30}\text{Zn}^{23+}$ ions

Hassan RAMADAN

*Basic Sciences Department, Faculty of Computer and Informations Sciences,
Ain Shams University, Cairo-EGYPT
e-mail: hramadan@eun.eg*

Received: 07.12.2010

Abstract

Resonant transfer and excitation (RTE) involving simultaneous electron capture and projectile L-shell excitation has been calculated for Fe^{19+} and Zn^{23+} ions, in charge states ranging from nitrogen-like to oxygen-like incident on molecular hydrogen over an energy range 0–250 MeV. By the same way the calculations have been performed with helium over an energy range 0–300 MeV. The calculations are carried out using the angular momentum average (AMA) scheme in the isolated resonance approximation (IRA). This method was previously used to calculate RTE cross sections for N-like P^{8+} and Ca^{13+} , where the results are found to agree with the present calculations. The present calculations are expected to serve as references for future comparison with experimental and theoretical works in different coupling schemes.

Key Words: Transition probability, resonant transfer excitation

1. Introduction

In ion-atom (I/A) collisions, a target electron may be captured by a positive ion projectile simultaneously causing the excitation of the projectile, leading to the formation of an intermediate doubly-excited state of the projectile. This process is known as resonant transfer excitation (RTE). The intermediate resonant doubly excited (d-states) of the projectile can then relax via the emission of x-ray. This process is called resonant transfer excitation followed by x-ray emission (RTEX). RTEX is analogous to the dielectronic recombination [1] (DR) process, in which the captured electron is initially free instead of bound.

Brandt [1] showed that RTEX in I/A collisions and dielectronic recombination (DR) in electron-ion (e/I) collisions are identical processes under the validity of conditions of impulse approximation (IMA). Brandt [1] proved that RTEX and DR cross sections are related through the Compton profile of the momentum distribution of electrons in molecular H_2 or atomic He targets.

The relationship between RTEX and DR cross sections is explored in many theoretical studies [2–4]. Many experimental [5, 6] and theoretical [7] studies have established the existence of RTE in ion-atom collisions.

Previous calculations of N-like ions P^{8+} and Ca^{13+} have been performed by Omar [8]. This was the motivation of the present work; which deals with the calculation of DR and RTECH cross sections for Fe^{19+} and Zn^{23+} as members of N-like ions. To avoid complexity, all Auger and radiative probabilities needed in DR and RTECH cross sections are calculated in the angular momentum average (AMA) scheme. In AMA scheme, all probabilities are averaged over both total orbital and total spin angular momenta for each intermediate d-state.

2. Theory

DR cross sections ($\bar{\sigma}^{DR}$) are calculated using the IMA within the framework of AMA to generate the RTECH cross sections ($\bar{\sigma}^{RTECH}$) for the collisions of Fe^{19+} and Zn^{23+} ions with H_2 and He targets. Bound states used in the calculations are obtained using the nonrelativistic single configuration Hartree-Fock (SCHF) approximation. The continuum wave functions are obtained using the distorted wave approximation (DWA).

All doubly excited intermediate states formed with $\Delta n \neq 0$ excitations and contributing to the ($\bar{\sigma}^{DR}$) cross sections are presented in Table 1, for 2s- and in Table 2, for 2p excitations.

Table 1. Intermediate d-states resulting from the 2s excitations of N-like ions with ground state configuration $1s^2 2s^2 2p^3$. The Auger and radiative decay channels are listed under headings of j-states and f-states

j-states	d-states ($\Delta n \neq 0$)	f-states
$1s^2 2s^2 2pn\ell n' \ell'$	$1s^2 2s^2 2p^3 n\ell n' \ell'$	$1s^2 2s^2 2p^2 n\ell n' \ell'$
$1s^2 2s^2 2p^2 n' \ell'$	(n = 3, 4)	$1s^2 2s^2 2p^3 n' \ell'$
$1s^2 2s^2 2p^2 n\ell$	($\ell = 0, 1, 2, 3$)	$1s^2 2s^2 2p^4 n' \ell'$
$1s^2 2s^2 2p^4$	($n' = 3, 4, 5$)	$1s^2 2s^2 2p^3 n'' \ell'' n' \ell'$
$1s^2 2s^2 2p^3 n'' \ell''$	($\ell' = 0, 1, 2, 3$)	$1s^2 2s^2 2p^3 n\ell$
		$1s^2 2s^2 2p^4 n\ell$
		$1s^2 2s^2 2p^3 n\ell n''' \ell'''$

Table 2. Same as Table 1, but for 2p excitation.

j-states	d-states ($\Delta n \neq 0$)	f-states
	$1s^2 2s^2 2p^2 n\ell n' \ell'$	$1s^2 2s^2 2p^3 n' \ell'$
$1s^2 2s^2 2p^2 n'' \ell''$	(n = 3, 4)	$1s^2 2s^2 2p^3 n\ell$
	($\ell = 0, 1, 2, 3$)	$1s^2 2s^2 2p^2 n'' \ell'' n\ell$
	($n' = 3, 4, 5, 6$)	$1s^2 2s^2 2p^2 n\ell n''' \ell'''$
	($\ell' = 0, 1, 2, 3$)	

Since the contributions from low-energy $\Delta n = 0$ intra shell excitations (L-shell excitations) to both DR and RTECH are not significant in the temperature range of interest, they are not included in this work.

The DR cross section ($\bar{\sigma}^{DR}$) is calculated by:

$$\bar{\sigma}^{DR} = \left[\frac{4\pi}{(p_0 a_0)^2} \right] \left(\frac{Ry}{\Delta e_c} \right) [\tau_0 V_a(i \rightarrow d)] \omega(d) (\pi(a_0)^2), \quad (1)$$

where $V_a(i \rightarrow d)$ and $\omega(d)$ are the radiationless capture probability and fluorescence yield, respectively, given by

$$V_a(i \rightarrow d) = \left(\frac{gd}{2gi} \right) \sum_{i_c, \ell_c} A_a(d \rightarrow i_c \ell_c) \quad (2)$$

and

$$\omega(d) = \frac{\sum_f A_r(d \rightarrow f)}{\Gamma_a(d) + \Gamma_r(d)}. \quad (3)$$

Here, the Auger and radiative transition probabilities A_a and A_r are the basic components of the cross section given by

$$\bar{A}_a = \left(\frac{2\pi e^2}{\hbar a_0} \right) \left| \langle i | \frac{1}{r_{12}} | d \rangle \right|^2 = \frac{2\pi}{\tau_0} \left| \langle i | \frac{1}{r_{12}} | d \rangle \right|^2, \quad (4)$$

and where $\tau_0 = 2.4189 \times 10^{-17}$ s is the atomic unit of time, a_0 is Bohr radius and $\frac{1}{r_{12}}$ is the electron-electron coupling operator.

On the other hand, the Auger width Γ_a is obtained by:

$$\bar{\Gamma}_a(d) = \left[\sum_{i, \ell_c} \bar{A}_a(d \rightarrow i, \ell) + \sum_{j, \ell'_c} \bar{A}_a(d \rightarrow j, \ell') \right] \quad (5)$$

The single-electron radiative probability is given by

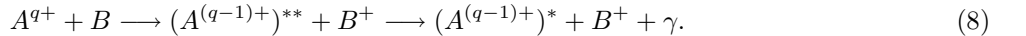
$$\bar{A}_r = \left(\frac{2\pi}{\hbar} \right) |\langle f | \hat{D} | d \rangle|^2 \rho_f, \quad (6)$$

where \hat{D} is the photon-electron interaction operator, and ρ_f is the density of final state.

Moreover, the radiative width Γ_r is given by summing all the radiative probabilities for all final states of the corresponding d-state:

$$\bar{\Gamma}_r(d) = \sum_f \bar{A}_r(d \rightarrow f). \quad (7)$$

Finally, the RTEK process can be represented schematically as



Atom B in the ion-atom collision plays no role in the RTEK process. The impulse approximation (IMA) is utilized to relate the RTEK cross section ($\bar{\sigma}^{\text{RTEK}}$) to the DR cross section ($\bar{\sigma}^{\text{DR}}$). The relationship between DR and RTEK cross sections, following Brandt [1] and Hahn [9] is given by

$$\bar{\sigma}^{\text{RTEK}} = \sqrt{\frac{M}{2E}} \Delta e_c J_B(p_z) \bar{\sigma}^{\text{DR}}, \quad (9)$$

where M is the mass of the projectile ion with energy E , $J_B(p_z)$ is the Compton profile and p_z is the z-component of the momentum.

3. Results and discussion

The RTE cross sections $\bar{\sigma}^{\text{RTEX}}$ are calculated for $\text{Fe}^{19+} + \text{H}_2$, $\text{Fe}^{19+} + \text{He}$, $\text{Zn}^{23+} + \text{H}_2$ and $\text{Zn}^{23+} + \text{He}$ collisions. $\bar{\sigma}^{\text{RTEX}}$ for $\text{Fe}^{19+} + \text{H}_2$ for 2s- and 2p excitations are shown in Figure 1. It is found that $\bar{\sigma}^{\text{RTEX}}$ for 2p excitation is about two times larger than that of the 2s excitation.

Figure 2 shows $\bar{\sigma}^{\text{RTEX}}$ for the collisions $\text{Fe}^{19+} + \text{H}_2$ and $\text{Fe}^{19+} + \text{He}$, where the RTE cross section for Fe^{19+} with He is broader than that for Fe^{19+} with H_2 . This reflects the nature of the Compton profile for the momentum distribution of the electrons in He target, which is broader than that of H_2 target.

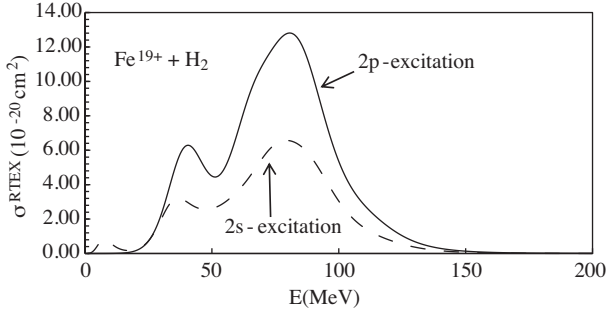


Figure 1. The variation of RTE cross section in units of cm^2 with the projectile Lab energy in units of MeV of the collision $\text{Fe}^{19+} + \text{H}_2$ for the 2s and 2p excitations.

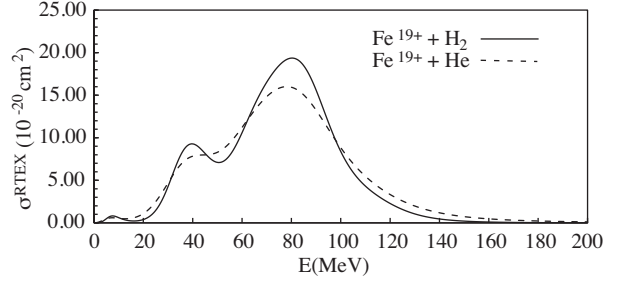


Figure 2. The variation of the RTE cross section in units of cm^2 with the projectile Lab energy in units of MeV for Fe^{19+} .

On the other hand, $\bar{\sigma}^{\text{RTEX}}$ for $\text{Zn}^{23+} + \text{H}_2$ and $\text{Zn}^{23+} + \text{He}$ are shown in Figure 3. These results are consistent with previous calculations [8] for P^{8+} and Ca^{13+} with H_2 and He targets (Figures 4 and 5). Although $\bar{\sigma}^{\text{RTEX}}$ for P^{8+} and Ca^{13+} show one peak behavior, the RTE cross sections for Fe^{19+} and Zn^{23+} show two maxima. These two maxima correspond to groups of intermediate resonance states in the RTE process for which the excited and the captured electrons occupy energy levels with quantum numbers $n = 3, 3$ or $n = 3, \geq 4$.

*

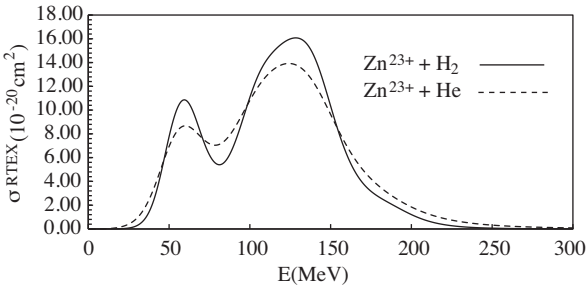


Figure 3. Same as Figure 2, but for Zn^{23+} .

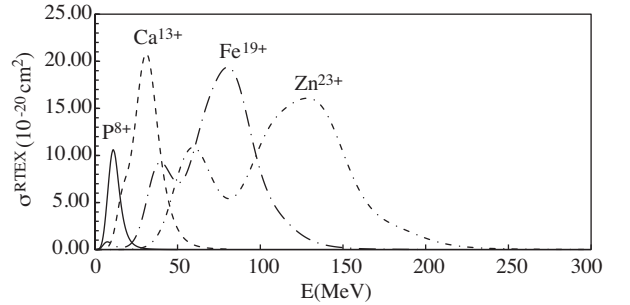


Figure 4. The RTE cross sections for P^{8+} , Ca^{13+} , Fe^{19+} and Zn^{23+} ions with H_2 .

The DR cross sections for the two ions Fe^{19+} and Zn^{23+} are given in Table 3, for each intermediate d-state with the corresponding continuum electron energy e_c .

*The notation $n = 3, 3$ and $n = 3, \geq 4$ refers to the principal quantum numbers of the intermediate excited states occupied by the two electrons which participate in the RTE process.

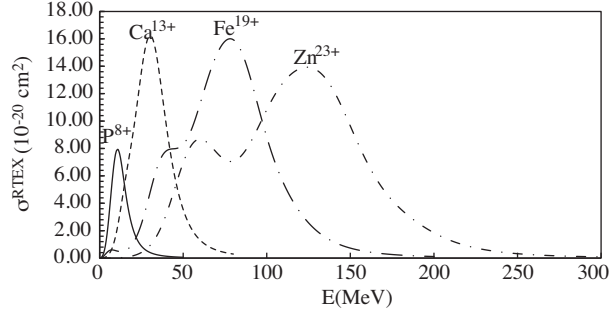


Figure 5. Same as Figure 3, but with He.

Table 3. The DR cross sections (in units of 10^{-20} cm^2) versus e_c (in Rydbergs) for 2s and 2p excitations.

2s excitation					2p excitation				
2*d-state	Fe^{19+}		Zn^{23+}		2*d-state	Fe^{19+}		Zn^{23+}	
	e_c	$\bar{\sigma}^{DR}$	e_c	$\bar{\sigma}^{DR}$		e_c	$\bar{\sigma}^{DR}$	e_c	$\bar{\sigma}^{DR}$
$1s^2 2s 2p^3 3s^2$	27.27	0.04	35.10	0.05	$1s^2 2s^2 2p^2 3s^2$	21.39	0.03	28.17	0.03
3s4s	46.94	0.15	63.78	0.09	3s4s	40.09	0.04	55.37	0.03
3s5s	56.03	0.1	76.62	0.09	3s5s	50.86	0.01	70.47	0.01
$\geq 3s6s$	60.7	0.2	83.25	0.18	3s6s	55.52	0.01	77.26	0.01
3s3p	28.12	1.11	36.27	1.25	$\geq 3s7s$	58.24	0.03	81.24	0.02
3s4p	42.42	0.87	56.68	1.00	3s3p	22.86	0.17	29.96	0.19
3s5p	5.82	0.63	68.95	0.7	3s4p	42.89	0.11	58.73	0.11
$\geq 3s6p$	55.24	1.29	75.44	1.42	3s5p	51.34	0.08	71.07	0.07
3s3d	25.6	3.75	31.76	4.55	3s6p	55.78	0.06	77.58	0.05
3s4d	43.5	1.48	57.99	1.62	$\geq 3s7p$	58.4	0.15	81.44	0.12
3s5d	51.34	0.93	69.59	0.96	3s3d	25.83	0.75	33.51	0.59
$\geq 3s6d$	55.53	1.89	75.8	1.95	3s4d	43.95	0.1	60.02	0.07
3s4f	44.3	0.53	58.99	0.54	3s5d	51.86	0.04	71.69	0.03
3s5f	57.44	0.3	70.06	0.35	3s6d	56.07	0.02	77.93	0.01
$\geq 3s6f$	61.48	0.60	76.06	0.71	$\geq 3s7d$	58.58	0.04	81.66	0.03
3p4s	48.63	0.53	65.23	0.59	3s4f	44.77	0.17	61.04	0.13
3p5s	58.23	0.29	79.11	0.30	3s5f	52.24	0.09	72.18	0.07
$\geq 3p6s$	63.04	0.58	86.11	0.61	3s6f	56.29	0.06	78.2	0.04
$3p^2$	31.08	0.02	39.71	0.02	$\geq 3s7f$	58.71	0.14	81.83	0.09
3p4p	48.65	0.02	65.54	0.03	3p4s	44.05	0.07	60.10	0.07
3p5p	58.99	0.01	80.12	0.02	3p5s	52.92	0.03	72.95	0.03
$\geq 3p6p$	63.43	0.03	86.63	0.03	3p6s	57.54	0.02	79.68	0.02
3p3d	33.61	0.63	42.75	0.75	$\geq 3p7s$	60.26	0.05	83.65	0.05
3p4d	51.65	0.18	69.14	0.19	$3p^2$	23.9	0.0004	31.46	0.0003
3p5d	59.53	0.1	80.77	0.1	3p4p	42.98	0.12	58.85	0.15
$\geq 3p6d$	63.73	0.20	86.99	0.20	3p5p	53.33	0.10	73.46	0.11
3p4f	52.44	0.68	70.12	0.62	3p6p	57.78	0.05	79.98	0.06
3p5f	59.00	0.41	81.24	0.35	$\geq 3p7p$	60.4	0.14	83.84	0.15

Table 3. Continued.

2s excitation					2p excitation				
2*d-state	Fe^{19+}		Zn^{23+}		2*d-state	Fe^{19+}		Zn^{23+}	
	e_c	$\bar{\sigma}^{DR}$	e_c	$\bar{\sigma}^{DR}$		e_c	$\bar{\sigma}^{DR}$	e_c	$\bar{\sigma}^{DR}$
$\geq 3p6f$	63.94	0.82	87.25	0.71	3p3d	27.91	4.37	36.03	5.01
3d5s	60.50	0.65	81.83	0.52	3p4d	45.99	1.16	62.47	1.24
$\geq 3d6s$	65.28	1.31	88.80	1.06	3p5d	53.88	0.51	74.12	0.54
3d4p	52.94	0.43	70.66	0.41	3p6d	58.08	0.28	80.34	0.29
3d5p	61.29	0.28	82.87	0.24	$\geq 3p7d$	60.59	0.70	84.06	0.73
$\geq 3d6p$	65.69	0.58	89.33	0.49	3p4f	46.80	0.63	63.47	0.60
3d ²	36.52	1.26	46.26	1.5	3p5f	54.26	0.30	74.59	0.29
3d4d	53.85	0.77	71.79	0.77	3p6f	58.29	0.17	80.61	0.16
3d5d	61.76	0.45	83.46	0.42	$\geq 3p7f$	60.72	0.42	84.23	0.40
$\geq 3d6p$	65.97	0.92	89.68	0.85	3d5s	55.22	0.09	75.70	0.05
3d4f	54.76	1.62	72.91	1.51	3d6s	59.82	0.05	82.40	0.03
3d5f	62.17	1.00	83.95	0.86	$\geq 3d7s$	62.52	0.12	86.36	0.07
$\geq 3d6f$	66.18	2.03	89.94	1.75	3d4p	47.29	2.22	64.01	2.07
4s ²	69.79	0.001	95.57	0.001	3d5p	55.66	1.36	76.23	1.11
4s5s	78.19	0.02	108.53	0.003	3d6p	60.07	0.88	82.71	0.66
$\geq 4s6s$	83.60	0.04	115.26	0.01	$\geq 3d7p$	62.67	2.21	86.55	1.66
4s4p	70.17	0.05	96.05	0.04	3d ²	30.85	6.06	39.57	7.01
4s5p	79.28	0.02	109.17	0.03	3d4d	48.21	4.83	65.15	4.7
$\geq 4s6p$	83.86	0.04	115.85	0.06	3d5d	56.14	3.07	76.83	2.74
4s3d	52.00	1.04	69.54	0.90	3d6d	60.34	2.17	83.05	1.77
4s4d	71.31	0.07	97.42	0.07	$\geq 3d7p$	62.85	5.47	86.76	4.46
4s5d	79.77	0.04	109.77	0.04	3d4f	49.15	4.29	66.29	3.78
$\geq 4s6d$	84.13	0.07	116.18	0.07	3d5f	56.55	2.86	77.34	2.33
4s4f	70.92	0.02	96.71	0.02	3d6f	60.57	1.97	83.33	1.51
4s5f	79.02	0.01	108.60	0.01	$\geq 3d7f$	62.98	4.96	86.93	3.80
$\geq 4s6f$	83.22	0.03	114.83	0.03	4s ²	64.13	0.004	88.90	0.003
4p5s	79.39	0.06	109.20	0.07	4s5s	72.15	0.0003	100.72	0.0003
$\geq 4p6s$	84.34	0.12	116.37	0.13	4s6s	77.22	0.0002	107.99	0.0002
4p ²	71.28	0.005	97.37	0.01	$\geq 4s7s$	80.21	0.001	112.29	0.0006
4p5p	80.02	0.0001	110.16	0.0001	4s4p	64.61	0.06	89.49	0.06
$\geq 4p6p$	84.71	0.003	116.88	0.0001	4s5p	73.74	0.003	102.63	0.003
4p4d	72.17	0.08	98.45	0.08	4s6p	78.33	0.002	109.32	0.002
4p5d	80.65	0.01	110.81	0.01	$\geq 4s7p$	81.01	0.01	113.26	0.01
$\geq 4p6d$	85.01	0.03	117.22	0.03	4s3d	44.49	0.24	60.64	0.15
4p4f	72.87	0.12	99.32	0.11	4s4d	65.76	0.002	90.87	0.02
4p5f	80.99	0.02	111.23	0.02	4s5d	74.24	0.001	103.23	0.001
$\geq 4p6f$	85.2	0.04	117.46	0.05	4s6d	78.60	0.0004	109.66	0.001
4d5p	81.06	0.02	111.29	0.02	$\geq 4s7d$	81.18	0.001	113.47	0.001
$\geq 4d6p$	85.6	0.04	117.93	0.04	4s4f	66.45	0.003	91.73	0.03
4d ²	73.22	0.12	99.73	0.15	4s5f	74.58	0.002	103.66	0.002
4d5d	81.47	0.06	111.66	0.01	4s6f	78.80	0.001	109.90	0.001

Table 3. Continued.

2s excitation					2p excitation				
2*d-state	Fe^{19+}		Zn^{23+}		2*d-state	Fe^{19+}		Zn^{23+}	
	e_c	$\bar{\sigma}^{DR}$	e_c	$\bar{\sigma}^{DR}$		e_c	$\bar{\sigma}^{DR}$	e_c	$\bar{\sigma}^{DR}$
$\geq 4d6d$	85.86	0.12	118.22	0.02	$\geq 4s7f$	81.30	0.003	113.62	0.004
4d4f	73.82	0.10	100.47	0.13	4p5s	74.14	0.005	103.11	0.005
4d5f	81.88	0.05	112.30	0.06	4p6s	78.91	0.004	110.01	0.004
$\geq 4d6f$	86.07	0.11	118.51	0.11	$\geq 4p7s$	81.68	0.01	114.06	0.01
4f5d	82.04	0.03	112.50	0.03	4p ²	65.38	0.06	90.50	0.07
$\geq 4f6d$	86.34	0.05	119.08	0.06	4p5p	73.40	0.02	102.23	0.03
4f ²	74.60	0.01	101.43	0.01	4p6p	79.13	0.02	110.29	0.02
4f5f	82.34	0.01	112.88	0.01	$\geq 4p7p$	81.82	0.06	114.24	0.06
$\geq 4f6f$	86.53	0.02	118.84	0.03	4p4d	66.56	0.49	91.85	0.45
					4p5d	75.06	0.08	104.23	0.08
					4p6d	79.42	0.05	110.64	0.05
					$\geq 4p7d$	82.00	0.12	114.45	0.13
					4p4f	67.29	0.17	92.74	0.13
					4p5f	75.40	0.01	104.65	0.01
					4p6f	79.62	0.01	110.89	0.01
					$\geq 4p7f$	82.12	0.02	114.6	0.03
					4d6s	79.78	0.002	111.07	0.002
					$\geq 4d7s$	82.55	0.004	115.10	0.004
					4d5p	75.46	0.12	104.71	0.12
					4d6p	80.02	0.10	111.36	0.09
					$\geq 4d7p$	82.70	0.25	115.28	0.23
					4d ²	67.62	0.67	93.13	0.78
					4d5d	75.88	0.38	105.08	0.09
					4d6d	80.27	0.29	111.68	0.27
					$\geq 4d7d$	82.86	0.74	115.48	0.67
					4d4f	68.24	0.23	93.90	0.29
					4d5f	76.30	0.16	105.74	0.16
					4d6f	80.49	0.14	111.94	0.13
					$\geq 4d7f$	82.99	0.35	115.64	0.33
					4f6p	80.51	0.01	111.96	0.01
					$\geq 4f7p$	83.17	0.03	115.87	0.03
					4f5d	76.47	0.06	105.95	0.07
					4f6d	80.78	0.04	112.30	0.04
					$\geq 4f7d$	83.46	0.11	116.23	0.11
					4f ²	69.05	0.02	94.89	0.02
					4f5f	76.78	0.02	106.34	0.02
					4f6f	80.95	0.02	112.55	0.02
					$\geq 4f7f$	83.34	0.04	116.08	0.04

4. Conclusion

The L-shell excitation cross sections are calculated for the RTE process in collisions of Fe¹⁹⁺ and Zn²³⁺ with H₂ and He targets. The DR cross sections for both 2s and 2p excitations are calculated in which the high Rydberg states (HRS) contribution is taken for $n \geq 6$ in case of 2s excitation and for $n \geq 7$ in case of 2p excitation. Where, this contribution is usually considered when \bar{A}_a 's and \bar{A}_r 's begin to scale as $1/n^3$. The results are summarized as follows:

- The RTE cross section for Fe¹⁹⁺ for 2p excitation is about two times larger than that for 2s excitation.
- σ^{RTE} shows two peak behavior for both Fe¹⁹⁺ and Zn²³⁺. This is attributed to different groups of intermediate resonance states in the RTE process for which the excited and the captured electrons occupy energy levels with quantum numbers $n = 3, 3$ or $n = 3, \geq 4$.
- The RTE cross sections exhibit a one peak behavior for P⁸⁺ and two overlapped peaks in case of Ca¹³⁺, Fe¹⁹⁺ and Zn²³⁺. So, it is expected that the two-peak behavior becomes more obvious for ions with $Z > 30$.
- The RTE cross sections for the collisions with He are broader than that with H₂, which reflects the nature of the Compton profile for the momentum distribution of the electrons in He target which is broader than that of H₂ target.

References

- [1] D. Brandt, *Phys. Rev.*, **A27**, (1983),1314.
- [2] Y. Hahn and H. Ramadan, *Phys. Rev.*, **A40**, (1989), 6206.
- [3] H. Ramadan and S. Elkilany, *Z. Naturforsch.*, **65a**, (2010), 599.
- [4] H. Ramadan, *Turk. J. Phys.*, **35**, (2011), 137.
- [5] P.F. Dittner, S. Datz, R. Hippler, H.F. Krause, P.D. Miller, P.L. Pepmiller, C.M. Fou, Y. Hahn, and I. Nasser, *Phys. Rev.*, **A38**, (1988), 2762.
- [6] V. Klimenko and T. F. Gallagher, *Phys. Rev.*, **A66**, (2002), 023401.
- [7] M.F. Gu, *Astro. J.*, **590**, (2003), 113.
- [8] G. Omar, H. Ramadan and T. El-Kafrawy, *Fisrt International Conference in Modern Trends in Physics Research, American Institute of Physics*, (2005),79.
- [9] Y. Hahn, *Adv. Atom & Molec. Phys.*, **21**, (1985), 123.